

MECHANICAL PROPERTIES OF GREEN CERAMIC BODIES

J.L. Amorós, E. Sánchez, V. Cantavella, M. Monzó

Instituto de Tecnología Cerámica (ITC)
Asociación de Investigación de las Industrias Cerámicas (AICE)
Universitat Jaume I. Castellón. Spain

G. Timellini

Centro Cerámico Bologna (CCB). Bologna. Italy

C.. Brindley

Ceram Research. Stoke-on-Trent. United Kingdom

1. ABSTRACT

The mechanical characterisation of green ceramic bodies has traditionally been restricted to determining bending strength. However, under certain conditions, pieces with relatively high bending strength can even give rise to a greater number of cracks and failure than those with lower mechanical strength.

Besides mechanical strength (σ_R), the present study also investigates other little used mechanical properties for characterising the mechanical performance of green ceramic bodies, such as Young's modulus (E) and, in particular, toughness (K_{IC}). Methods are proposed for measuring these properties and the effect of spray-dried powder variables on these properties is analysed.

2. INTRODUCTION

Green mechanical properties are of singular importance in the ceramic tile manufacturing process. The absence of good mechanical properties leads to rejects (both in the green and fired product), with the ensuing cost involved in reuse in the production process or disposal and resulting environmental impact.

The reject percentage associated with cracking and failure is estimated at around 3%; while the fired reject caused by cracks in the green ware is about 2%. This means that just in Europe, the economic losses associated with cracking and failure in green materials can be assessed at around 170 million euros. It is therefore obvious that even a minor decrease in flawed green tile would entail significant economic savings.

The problem of fracture in green material is aggravated by the current tendency to produce ever-larger sizes. Thus, part of the study conducted has highlighted the important rise in rejects caused by working with large sizes.

Mechanical strength has been practically the sole property used to analyse the mechanical behaviour of green ceramic bodies. However, this mechanical property is insufficient to understand this behaviour. Thus, completely dry tiles have sometimes been found to fail more than when they exhibit a certain residual moisture, even though the mechanical strength of perfectly dry tiles is greater.

The foregoing led to proposing a study, within the framework of the programme for Industrial Technologies and Materials (Brite-Euram III), designed to improve tile mechanical properties. The results set out in this paper report part of the findings from this European project.

The fact that mechanical strength is inadequate to fully characterise the mechanical properties of green ceramic materials gave rise to a search for other, complementary properties, which would yield a better understanding of fracture in materials. In fired technical ceramics, besides mechanical strength, other mechanical properties such as Young's modulus and toughness are also used.

Young's modulus measures a material's rigidity. The more rigid a material, the higher its modulus of elasticity. A material is considered to exhibit brittle fracture if its behaviour is elastic virtually up to failure. Young's modulus does not depend on faults (microcracks) in the material.

Toughness, on the other hand, is a measure of a material's resistance to crack propagation. Unlike mechanical strength, toughness is independent of fracture-initiating flaws (microcracks), though it depends on the microstructure of the material.

Though there are methods for determining the foregoing mechanical properties in fired ceramic materials, very few studies have been undertaken on the application of these methods to green materials ^[1-6].

-
- [1] AMORÓS, J.L.; FELIU, C.; GINÉS, F.; AGRAMUNT, J.V.; *Mechanical strength and microstructure of green ceramic bodies*. In: Qualicer, IV World Congress on Ceramic Tile Quality, Castellón: Cámara Oficial de Comercio, Industria y Navegación. 1996, vol. I, p.153-171.
 - [2] KENDALL, K. *The Strength of Green Bodies*. In HOWLETT, S.P., TAYLOR, D. eds. Special Ceramics 8. Stoke-on-Trent: The Institute of Ceramics, 1986, p.255-265.
 - [3] ABDEL-GHANI, M. ET AL. *Mechanical Properties of Cohesive Particulate Solids*. Powder Technol., 65, 113-123, 1991.
 - [4] BORTZMEYER, D. ET AL. *Fracture Mechanics of Green Products*. J. Eur. Ceram. Soc., 11, 9-16, 1993.
 - [5] THOMPSON, R.A. *Mechanics of Powder Pressing: III, Model for the Green Strength of Pressed Powders*. Am. Ceram. Soc. Bull. 60(2), 248-251, 1981.
 - [6] RUMP, H. *Zur Theorie der Zugfestigkeit von Agglomeraten bei Kraftübertragung an Kontaktpunkten*. Chem-Ing. Techn., 42(8), 538-540, 1970.

The present work analyses several methods for measuring the different properties and undertakes to determine how the spray-dried powder variables and the forming process affect these properties.

3 FRACTURE MECHANISM

Ceramic materials exhibit “flaws” (microcracks) that act as stress-focussing elements, which determine the points at which material fracture starts. Tile failure therefore depends on flaw distribution and size. As a random distribution is involved, the mechanical strength measurement exhibits scattering^[7]. The mean mechanical strength value is insufficient to characterise the mechanical strength of a tile; it is necessary to take into account the scatter. This mechanical strength distribution is quantitatively given by the Weibull distribution^[8, 9], defined by parameter “m”. As m rises, the scatter in the mechanical strength data decreases.

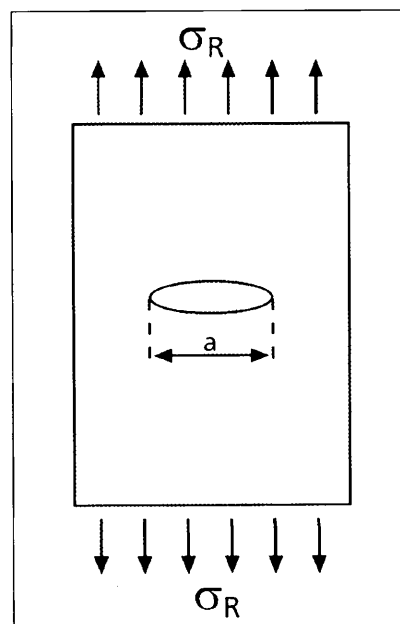


Figure 1. Elliptical crack model analysed by Irwin.

Mechanical strength depends on two factors: intrinsic material characteristics (including material microstructure) and the presence of microcracks. The theoretical calculation of fracture resistance can be tackled from two different standpoints: an approximation in terms of energy (Griffith analysis) and an approximation in terms of stress (Irwin analysis). If material behaviour is elastic, both approximations are equivalent.

The Irwin analysis yields the following equation for the mechanical strength (σ_R) of a test specimen with an unbounded extension and an elliptical microcrack of semi-length “a” (Figure 1), subject to pure tensile stress:

$$\text{Eq. 1} \quad \sigma_R = \frac{K_{IC}}{\sqrt{\pi a}}$$

where K_{IC} is a characteristic material constant known as toughness. In practice, specimens are not of unbounded length and stress is not constant (as in the case of the 3 and 4-point bend tests). The foregoing equation is therefore usually rewritten as:

$$\text{Eq. 2} \quad \sigma_R = \frac{K_{IC}}{Y\sqrt{a}} \quad \text{or} \quad \text{Eq. 3} \quad K_{IC} = \sigma_R Y \sqrt{a}$$

where Y is a dimensionless constant that depends on flaw size.

It can be observed in Eq. (2) that mechanical strength decreases as flaw size rises. In other words, specimens with larger microcracks will present lower mechanical strength.

[7] TORRECILLAS, R.; MOYA, J.S. *Mecánica de Fractura en Materiales Cerámicos Frágiles. I: Principios Fundamentales*. Bol. Soc. Esp. Ceram. Vidr. 27, 123-135, 1988.

[8] DAVIES, D.G.S. *The Statistical Approach to Engineering Design in Ceramics*. Proc. Br. Ceram. Soc., 21, 429-452, 1973.

[9] PAPARGYRIS. *Estimator Type and Population Size for Estimating the Weibull Modulus in Ceramics*. J. Eur. Ceram. Soc., 18, 451-455, 1998.

4. EXPERIMENTAL

4.1.- TEST SPECIMEN PREPARATION

The experiments run to determine the mechanical properties were conducted with test specimens made from an industrial, spray-dried powder usually employed for making redware floor tile.

Test specimens measuring 80 mm x 20 mm, with variable thickness (depending on the test method used), were made by uniaxial pressing on an automatic laboratory press.

4.2.- TEST SPECIMEN CHARACTERISATION

Specimen bulk density (ρ) was measured by the mercury immersion method.

Pore size was determined on a Micromeritics, Model AutoPore III 9420, mercury porosimeter at a maximum pressure of 30,000 psi.

Specimen fracture appearance was observed with a Philips, Model XL30EI, electronic microscope.

The mechanical tests were performed on an Instron, Model 6027, universal mechanical testing machine, working with a load cell of 1 kN. Mechanical strength was determined by 3 and 4-point bend tests and diametral compression. Young's modulus was measured by 3 and 4-point bend tests, and finally, toughness was measured by bending tests with notched specimens. All these tests are described in further detail below.

The mechanical strength data were analysed by means of the Weibull equation. This equation relates a specimens' survival probability (p_s) to the stress undergone (σ_R):

$$\text{Eq.4} \quad p_s(\sigma_R) = \exp \left[- \left(\frac{\sigma_R}{\sigma_0} \right)^m V_E \right]$$

where:

p_s : survival probability (probability of a specimen undergoing maximum stress σ_R without fracturing).

σ_0 : scale parameter (MPa)

V_E : equivalent volume (m^3)

m : dimensionless constant (Weibull modulus)

V_E depends on specimen volume and the way the load is applied (3-point, 4-point

[10] MARION, R.H.; Johnstone, J.K. *A Parametric Study of the Diametral Compression Test fo Ceramics*. Am. Ceram. Soc. Bull., 56(11), 998-1002, 1977.

bending, etc.). Constant m characterises the mechanical strength measurement scatter. As m rises, scatter decreases. Plotting $\ln \ln(1/p_S)$ versus $\ln \sigma_R$ yields a straight line of slope m . The following expression can be readily derived from Eq. 4:

$$\text{Eq. 5} \quad \ln \ln \frac{1}{p_S} = m \ln \sigma_R + (\ln V_E - m \ln \sigma_0)$$

5. RESULTS AND DISCUSSION

5.1 SELECTION OF THE PROCEDURE FOR DETERMINING MECHANICAL PROPERTIES

5.1.1 Mechanical strength

—Description of test methods

Three mechanical strength measurement methods were analysed: 3-point bending (3PB) (Figure 3)^[11], 4-point bending (4PB) (Figure 4) and diametral compression (DC) (Figure 5).

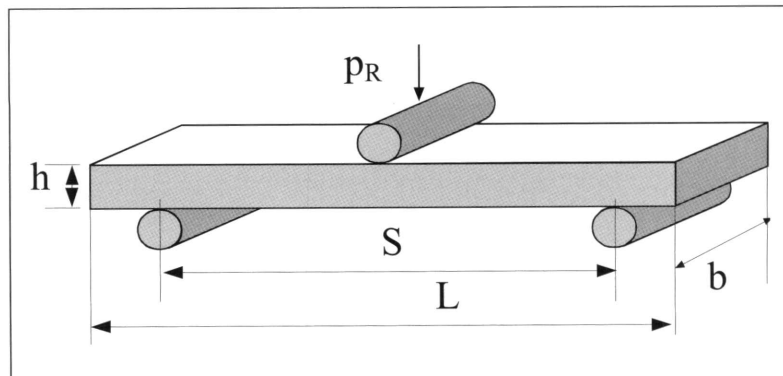


Figure 3. Schematic illustration of 3-point bending configuration.

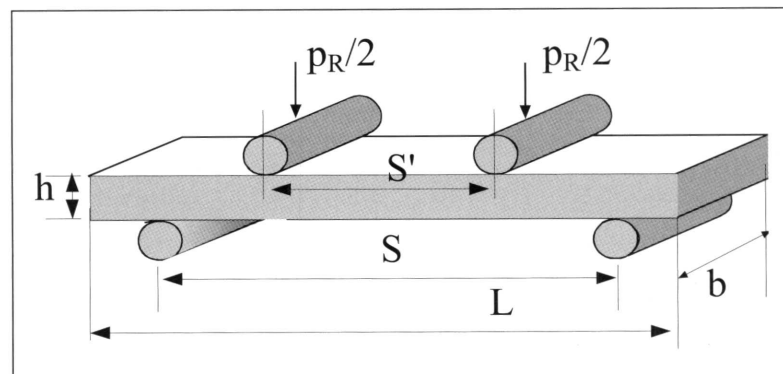


Figure 4. Schematic illustration of 4-point bending configuration.

[11] NEGRE, F.; SÁNCHEZ, E.; GINÉS, F.; GARCÍA, J.; FELIU, C.. *Procedimiento experimental para determinar la resistencia mecánica mediante flexión por tres puntos de apoyo*. *Técnica Cerámica*, 225, 452-463, 1994.

Method	Equation	
3-point bending (3PB)	$\sigma_R = \frac{3}{2} \frac{S}{bh^2} p_R$	Ec. 6
4-point bending (4PB)	$\sigma_R = \frac{3}{2} \frac{S - S'}{bh^2} p_R$	Ec. 7
Diametral compression (DCD)	$\sigma_R = \frac{2}{\pi} \frac{1}{Dh} p_R$	Ec. 8
Diametral compression with padding (DCP)	$\sigma_R = \frac{2}{\pi} \frac{p_R}{Dh} \left(1 - \frac{7}{6} \left(\frac{w}{D} \right)^2 \right) (*)$	Ec. 9

(*) This equation is only valid for small values of the w/D ratio.

Table 1. Equations used for determining mechanical strength.

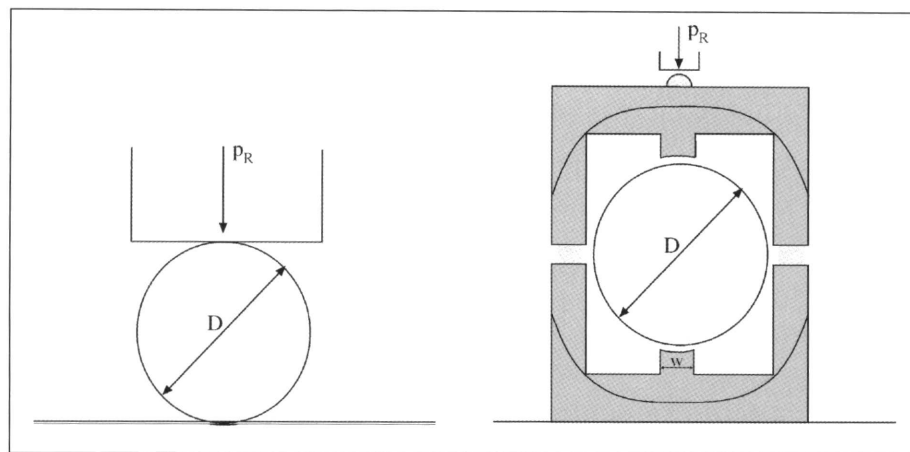


Figure 5. Schematic illustration of the diametral compression configuration with direct load application (left) and with padding (right).

In the bending methods, the specimen with a parallelepiped shape was placed on two supporting rods, and the force was applied through one top load rod (3PB) or two top load rods (4PB).

In the diametral compression test, the specimen is disk-shaped and loading takes place at two diametrically opposite points. This produces high compression stress at these two points and sometimes failure occurs close to these points instead of arising in the centre of the test specimen. For this reason, besides considering the diametral compression test with direct force application (DCD), an assembly was designed in which the load was applied via pads that distributed the force and avoided focussing it at one point (DCP) (Figure 5).

Table 1 presents the equations used to calculate mechanical strength (σ_R) with the methods set out above (the symbols are described in the corresponding figures).

Table 2 lists the results from the 3 and 4-point bend tests and the diametral compression tests (with and without padding) of the dry test specimens, indicating pressing pressure (p) and moisture content (X_p) of the spray-dried powder used for

making the specimens, mean mechanical strength ($\bar{\sigma}_R$) and the relation between mechanical strength standard deviation (s) and mean mechanical strength. For the 3PB and 4PB tests, the Weibull modulus (m) is also included.

Method	p (MPa)	X_p (%)	$\bar{\sigma}_R$ (MPa)	$s / \bar{\sigma}_R$ (%)	m	
3PB	15	3	1.10	2.86	42	
		7	3.10	3.46	35	
	60	3	3.37	3.34	35	
		7	6.30	4.22	29	
4PB	15	3	0.970	5.65	20	
		7	2.97	4.24	28	
	60	3	3.25	5.46	21	
		7	6.37	4.36	27	
	DCD	15	3	0.497	4.29	--
			7	1.51	2.95	--
60		3	1.57	3.98	--	
		7	2.79	4.01	--	
DCP	15	3	0.591	5.55	--	
		7	1.80	2.29	--	
	60	3	2.00	5.41	--	
		7	3.74	4.16	--	

Table 2. Mean mechanical strength ($\bar{\sigma}_R$) and Weibull modulus (m) obtained in the different mechanical strength tests.

The 3PB and 4PB tests yielded similar values for $\bar{\sigma}_R$. This is indicative of a high Weibull modulus in the specimens. Thus, the scatter in mechanical strength in 4PB (lower value for m than in 3PB) cannot be just a consequence of the characteristics of the material, but will possibly be the result of the assembly itself or test specimen preparation. In fact, subsequent study revealed the existence of small variations in density and thickness throughout the length of the specimen. These variations are more critical in 4PB than in 3PB, in which maximum stress is focussed at the centre of the specimen.

The diametral compression tests yielded clearly lower mechanical strength values than the bending tests. This phenomenon was originally attributed to fracture arising at the contact points between the specimen and the support, as happens with fired ceramic materials [12]. To establish to what extent this might be the cause of the lower mechanical strength, a support was designed that distributed the applied force over a given surface (DCP test). The results obtained with the dry specimens indicate a slight rise in mechanical strength, which was however far removed from the values reached in bending. This suggests that there is either some other factor that diminishes mechanical strength in diametral compression, or that the pads did not wholly manage to correct the problem.

When the mechanical test was performed on moist specimens (as-pressed), similar results were found in 3PB and 4PB compared to those with the dry specimens. However in diametral compression, the difference in mechanical strength found between diametral compression with padding (DCP) and without padding (DCD) decreased. The explanation for this phenomenon could lie in the pseudoplastic behaviour of the as-pressed specimens. Owing to their moisture content, the specimens tested in DCD deformed readily at their point of contact, so that this deformation acted as “natural padding”.

[12] RUDNICK, A.; HUNTER, A.R.; HOLDEN, F.C. *An Analysis of the Diametral-Compression Test. Materials Research and Standards*, 283-289, 1963.

The determination of the Weibull modulus from the diametral compression tests is more delicate than when working with bending, and requires using a multiaxial Weibull formula [13,14]. For this reason, only tensile, compression or bending tests are normally used to determine the Weibull modulus.

— *Selecting the most appropriate method*

Owing to the smaller scatter in the σ_R values found in 3PB compared to 4PB, the 3PB test is considered preferable to the 4PB test.

The data scatter found in the diametral compression of the dry specimens was comparable to that exhibited by 3PB, but diametral compression yielded much lower mechanical strength. Furthermore, the fact that diametral compression is a test involving multiaxial stress entails a series of difficulties on statistically processing mechanical strength. Thus, 3PB is considered preferable to diametral compression. However, the ease of preparation of diametral compression test specimens, and the correlation between 3PB and diametral compression test data make this a good industrial mechanical strength control method.

5.1.2 Young's modulus

— *Description of the test methods*

Young's modulus is usually determined from the load curve (p) versus the displacement at the load application point (y). If the behaviour is elastic, the plot $p=p(y)$ should be a straight line (Figure 6), from whose slope E can be calculated. Table 3 presents the equations used to calculate the modulus of elasticity in the 3PB and 4PB tests.

Method	Equation	
3-point bending (3PB)	$p = \frac{4bh^3E}{S^3} y$	Ec. 10
4-point bending (4PB)	$p = \frac{4bh^3E}{(S-S')^2(S+2S')} y$	Ec. 11

Table 3. Equations used for determining mechanical strength.

p (MPa)	X_p (%)	3-point bending		4-point bending	
		\bar{E} (GPa)	s/\bar{E} (%)	\bar{E} (GPa)	s/\bar{E} (%)
15	3	1.73	3.82	1.47	19.5
	7	3.56	3.80	3.41	4.75
60	3	3.59	2.60	3.08	18.2
	7	5.41	5.51	5.30	3.56

Table 4. Mean Young's modulus (\bar{E}) determined from dry 3PB and 4PB tests.

Table 4 presents Young's modulus for the dry specimens. As expected, Young's modulus rises on raising pressing pressure and moisture content.

[13] VARDAR, O; FINNIE, I. *An analysis of the Brazilian disk fracture using the Weibull probabilistic treatment of brittle strength. Int. Journ. of Fracture*, 11, 495-508, 1975.

[14] KERKHOFF, F. *Fundamentals of the Mechanical Strength and the Fracture Mechanics of Ceramics. En Ceramic Monograph. Handbook of Ceramics. Freiburg: Schmid, Part 3.1.1., p. 1-13, 1993.*

The modulus of elasticity calculated from the 4PB tests exhibit a clearly greater scatter (s/\bar{E}) than in the 3PB tests. This outcome matches the greater scatter found on performing the 4PB test $s/\bar{\sigma}_{Rv}$ and indicates the presence of small experimental errors in the assembly or specimen preparation, which are less significant in 3PB.

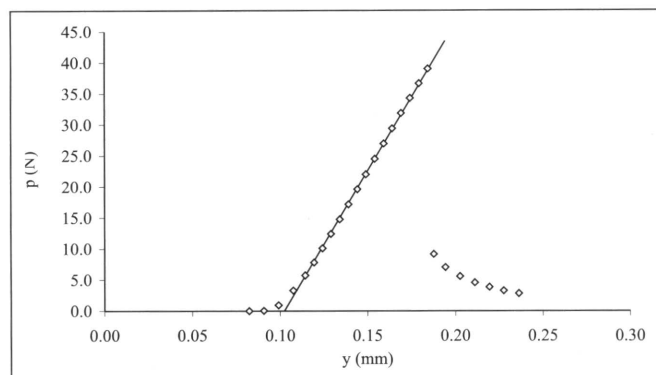


Figure 6. Load-displacement curve and obtainment of the slope for calculating Young's modulus.

— Selection of the most appropriate method

In view of the results detailed in the foregoing tables, the 3-point bend test is recommended for calculating Young's modulus, as it exhibits less data scatter.

5.1.3 Toughness

Many toughness measurement methods use specimen notching^[14,15]. The notch acts as the "fracture-initiating flaw" and entails the advantage, compared to natural faults, of being able to measure it accurately.

Other toughness measurement methods such as the indentation methods^[16] do not appear to be readily applicable to green ceramic bodies. Moreover, they lead to parameters that need to be related by empirical equations to toughness, yielding different results depending on the equation used.

The methods analysed for measuring toughness differ with regard to the shape of the notch made and the system used to make it.

— Applicability of the toughness concept to green ceramic bodies

The toughness measurement methods using notching are based on Eq. (3) (or an expression derived from this equation). If notches of differing thickness are made (a_1, a_2, \dots, a_i), yielding different apparent mechanical strengths ($\sigma_{R1}, \sigma_{R2}, \dots, \sigma_{Ri}$), Eq. (2) can be rewritten as:

Eq. 12

$$\sigma_{Ri} = \frac{K_{IC}}{Y(a_i)\sqrt{a_i}}$$

[14] KERKHOFF, F. *Fundamentals of the Mechanical Strength and the Fracture Mechanics of Ceramics*. En Ceramic Monograph. Handbook of Ceramics. Freiburg: Schmid, Part 3.1.1., p. 1-13, 1993

[15] TORRECILLAS, R.; MOLLA, J.S. *Mecánica de Fractura en Materiales Cerámicos Frágiles. II. Propagación Subcrítica de grietas*. Bol. Soc. Esp. Ceram. Vidr. 28, 123-135, 1988.

[16] SESHADRI, S.G.; SRINIVASAN, M.; KING, L. *Indentation Fracture Testing of Ceramics*. Ceram. Eng. Sci. Proc. 4(9-10), 853-863, 1983.

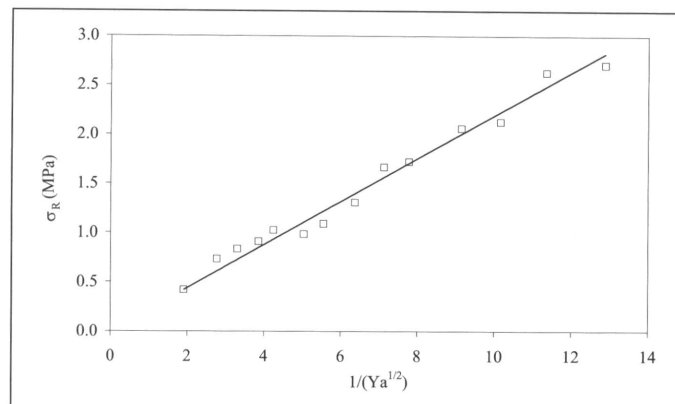


Figure 7. Plot of mechanical strength versus $1/(Ya^{1/2})$.

Therefore, the plot of σ_{Ri} versus $1/(Y(a_i)a_i^{1/2})$ should be a straight line [17]. Figure 7 plots the experimental values of σ_R versus $1/(Ya^{1/2})$.

The resulting plot is linear, which means that K_{IC} can be considered a characteristic parameter of material behaviour (independently of notch size), justifying its use in analysing the fracture mechanism.

If the size of the natural flaw is comparable to that of the notch, it is necessary to make a series of corrections to Eq. (12), but the method is equally applicable.

—Description of the test method

Three methods were used to determine toughness:

- Straight part-through notch cut with a disc (SPD): a parallelepiped test specimen is used and a straight part-through notch is made with a diamond disk (Figure 8.A)
- Straight part-through notch cut with a blade (SPC): the test specimen is formed in a mould containing a blade that produces the notch. This method allows making finer notches than with SPD.
- Chevron (triangular) notch cut with a disc (STD): this is similar to the SPD method, but the notch has a triangular shape. In principle this method is less sensitive to notch width (Figure 8.B)[18].

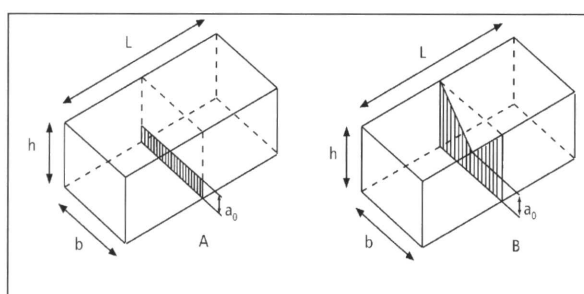


Figure 8. Straight part-through (A) and triangular (B) notches.

[17] MULLIER, M.A.; SEVILLE, J.P.K.; ADAMS, M.J. *A Fracture Mechanics Approach to the Breakage of Particle Agglomerates*. Chem. Eng. Sci. 42(4), 667-677, 1987.
 [18] MUNZ, D.; BUBSEY, R.T.; SHANNON, J.L. *Fracture Toughness Determination of Al₂O₃ Using Four-Point-Bend Specimen with Straight-Through and Chevron Notches*. J. Am. Ceram. Soc. 63(5-6), 300-305, 1980.

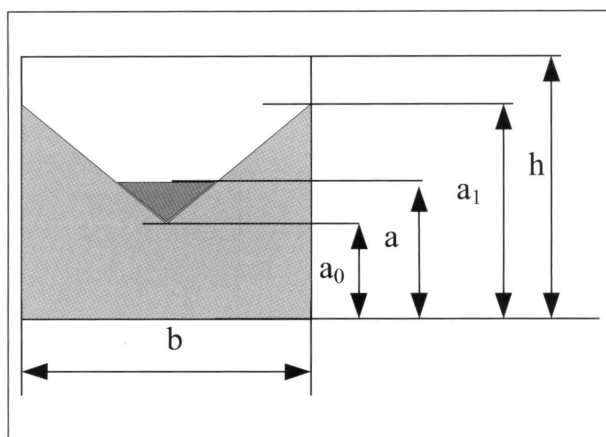


Figure 9. Characteristics dimensions of the chevron notch made.

In the two first methods, a series of parallelepiped test specimens was made with a straight part-through notch of depth $\alpha = a_0/h \approx 0.4$ (40% of total thickness). Toughness was determined from Eq. (3), where σ_R was given by Eq. (7).

Figure 9 presents the characteristic chevron notch dimensions. A series of parallelepiped test specimens was made, subsequently making the chevron notch with the following geometry: $\alpha_1 = a_1/h = 1.0$, $\alpha_0 = a_0/h = 0.2$. The specimens were 20 mm wide and (approximately) 12 mm thick. After forming they underwent 3PB testing.

Toughness was calculated from:

Eq. 13
$$K_{IC} = \frac{P_{max}}{b\sqrt{h}} Y_{min}^*$$

where Y_{min}^* is a parameter that can be derived from the load-deformation curve.

Method	p (MPa)	X_p (%)	K_{IC} (MPa m ^{1/2})	s/ K_{IC} (%)
SPD	15	3	0.0181	43
	60	7	0.205	4.9
SPC	15	3	0.0227	20
	60	7	0.193	15
STD	15	3	0.0412	3.1
	60	7	0.264	8.6

Table 5. K_{IC} obtained with the straight part-through notch (disc).

Table 5 details the toughness values obtained using the different methods chosen. The table lists the pressing pressure (p), pressing moisture content (X_p), toughness (K_{IC}) and scatter relative to the toughness data (s/ K_{IC}).

— Selection of the most appropriate method

The selection of the most appropriate method for measuring toughness was mainly based on two criteria: ease of test performance and low data scatter.

With regard to the first criterion, the most suitable method would be the first one (SPD). However, owing to the low mechanical strength of the green material, the data scatter was very large (especially at low pressing pressure and moisture content), making this method inadvisable.

The SPC method exhibited lower scatter of the K_{IC} data (at low mechanical strength values), though it involved the disadvantage of long test specimen preparation time.

The chevron notch method (STD) uses test specimens that are relatively easy to make, and yielded clearly better K_{IC} data scatter. This method is therefore considered the most appropriate one for determining mechanical strength.

After selecting the method from the dry specimen data, the validity of method was tested on the as-pressed specimens. The satisfactory outcomes verified that the method could be applied with equal accuracy to the as-pressed test specimens.

5.2.- INFLUENCE OF PROCESS VARIABLES ON TEST SPECIMEN CHARACTERISTICS

5.2.1 Pore-size distribution

Table 6 lists the data obtained in the mercury porosimetry tests: 50% pore diameter (by volume)(D_{50}) and true porosity (ϵ).

It can be observed in the first place that pore size was clearly smaller than the flaw size (microcrack) calculated from the fracture mechanics equations. This means that the pores are not responsible for the fracture-generating flaws, but that flaw size is possibly related to granule dimensions.

The evolution exhibited by both parameters was as expected: D_{50} and ϵ decreased when pressing pressure and moisture content rose.

p (MPa)	X_p (%)	D_{50} (nm)	ϵ (%)
15	3	233	18.9
	5	194	16.7
	7	147	14.4
30	3	139	14.6
	5	104	12.7
	7	76.9	11.2
60	3	88.2	12.1
	5	65.7	10.1
	7	43.6	8.7

Table 6. Values of D_{50} and porosity (ϵ) in terms of pressing pressure (p) and spray-dried powder moisture content (X_p).

5.2.2 Observation of fracture appearance

Figure 10 shows the appearance of the fracture exhibited by the specimens pressed at a pressure of 15 MPa and moisture content of 3%. At these pressure and moisture content values, granules can be observed at the fracture surface. This is because during pressing, the pressure was not high enough to break up the granules, and fracture propagated through the weakest region, i.e., through the intergranular region.

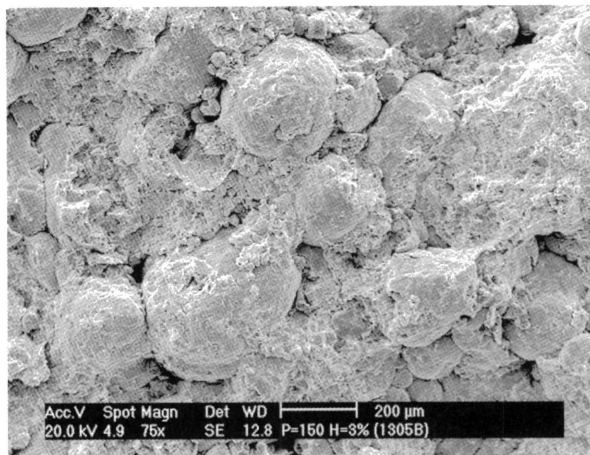


Figure 10. Fracture appearance in the test specimen formed at $p=15$ MPa, $X_p=3\%$

On raising pressure and moisture content (Figure 11), granule identity disappears, even though some granule contours can still be distinguished. Fracture proceeds between granule rests and through the granules.

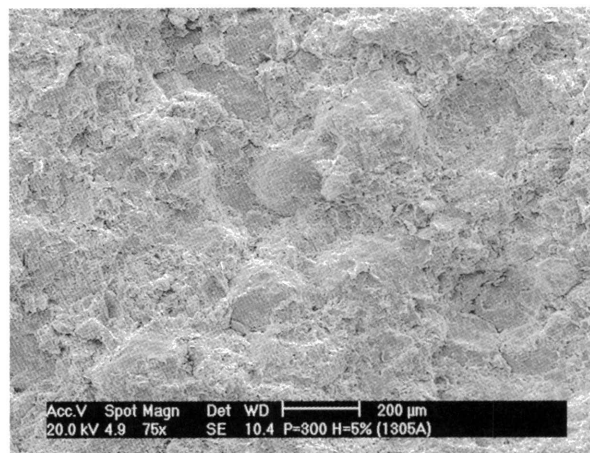


Figure 11 Fracture appearance in the test specimen formed at $p=30$ MPa, $X_p=5\%$

5.3.- INFLUENCE OF PROCESS VARIABLES ON MECHANICAL PROPERTIES

5.3.1 Effect of moisture content and pressing pressure

—Mechanical strength

Figure 13 plots mechanical strength as a function of spray-dried powder density and moisture content. The plot shows that mechanical strength rises with pressing pressure and moisture content. This effect can be explained by considering that as density increases (and porosity decreases), interparticle contacts rise, making separation and hence specimen failure more difficult.

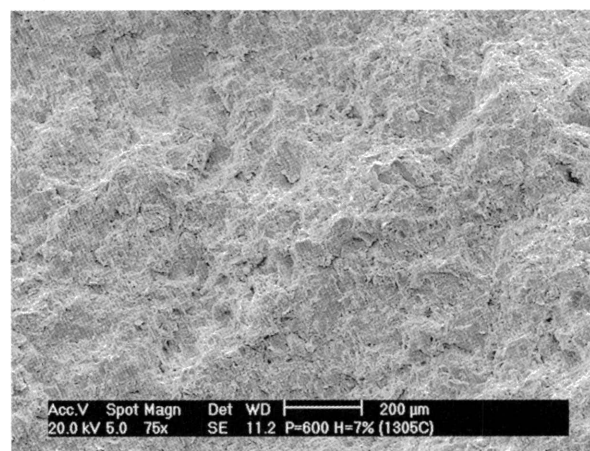


Figure 12. Fracture appearance in the test specimen formed at $p=30$ MPa, $X_p=7\%$

On the other hand, at the same density, mechanical strength rises slightly on raising moisture content. The rise of mechanical strength with moisture content (at a fixed bulk density) is usually considered to be due to the plasticising effect of water: as agglomerate moisture content is raised, the agglomerates become more readily deformable, so that particle packing could become more stable.

– Young’s modulus

Figure 14 plots the values of Young’s modulus (E) as a function of pressing pressure (p) and spray-dried powder moisture content (X_p).

The modulus of elasticity parallels the behaviour of mechanical strength with pressing pressure and moisture content, by rising with pressing pressure and spray-dried powder moisture content.

– Toughness

Figure 15 plots the evolution of K_{IC} , calculated from the SENB method with a chevron notch and Figure 16 presents the evolution of the size of the natural flaw (a').

The variation of K_{IC} with density, pressure and moisture content is, to a certain extent, similar to that of σ_R . However, at a given bulk density, K_{IC} is more sensitive than σ_R to variations in moisture content or pressing pressure. The reason for the variation of K_{IC} with ρ , p and X_p could in principle be qualitatively similar to the reason for the variation of σ_R . However, to

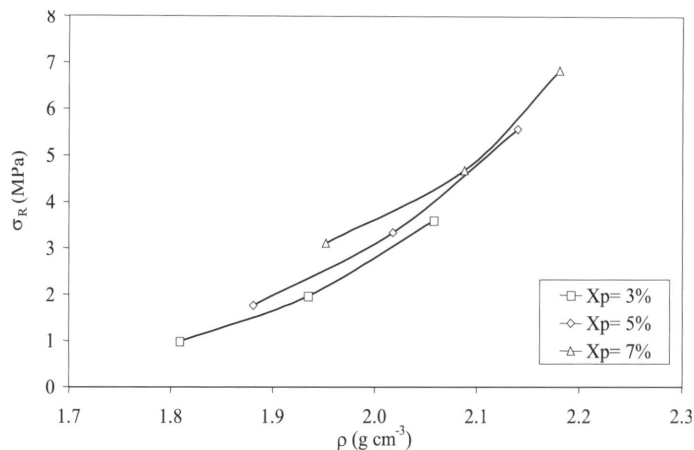


Figure 13. Evolution of mechanical strength with bulk density at different pressing pressures.

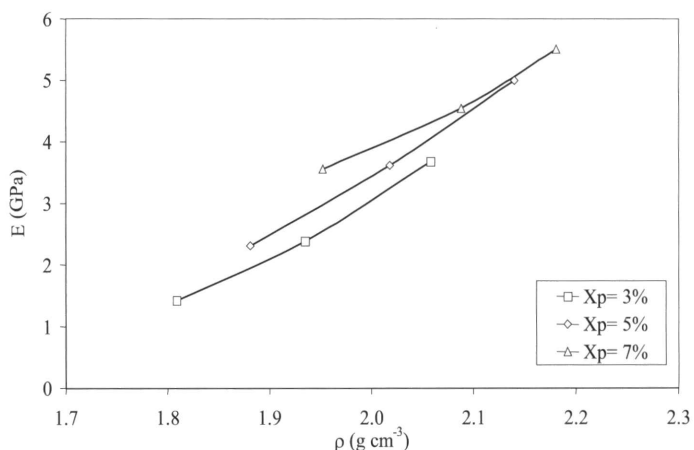


Figure 14. Evolution of Young’s modulus with bulk density at different pressing moisture contents.

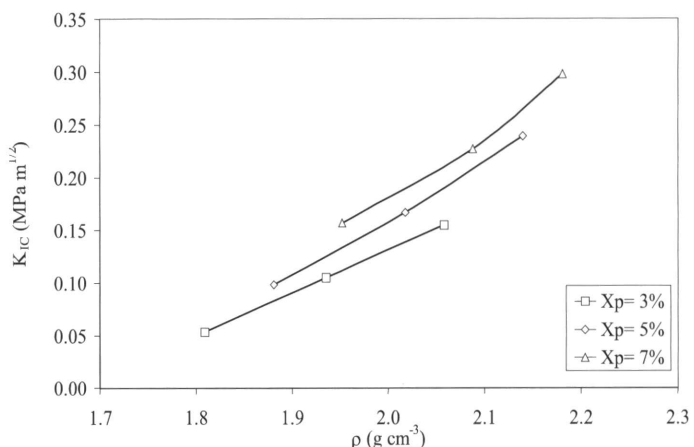


Figure 15. Evolution of toughness with bulk density at different pressing moisture contents.

understand its quantitative evolution it is necessary to take into account the change in size of the natural flaw with bulk density (Figure 16), which decreases on raising this variable.

The fact that at a fixed bulk density, K_{IC} is more sensitive than mechanical strength can be explained by using linear fracture mechanics equations.

5.3.2 Effect of granule size

Table 7 presents the mechanical strength, Young's modulus and toughness data for the two studied particle-size fractions: $100 < D < 200 \mu\text{m}$ and $400 < D < 500 \mu\text{m}$. For comparative purposes, it also includes the relative difference between the properties of the two fractions (Δ).

Fraction	ρ (g cm ⁻³)	σ_R (MPa)	E (GPa)	K_{IC} (MPa m ^{1/2})	a' (μm)
100-200 μm	2.026	3.56	3.20	0.187	720
400-500 μm	2.035	3.07	3.44	0.178	875
Δ (%)	--	-15 %	7 %	- 5%	19 %

Table 7. Mechanical strength (σ_R) Young's modulus (E) and toughness (K_{IC}) of the specimens prepared with the studied granule-fractions.

The highest mechanical strength values were found with the smaller granule-size fraction. Young's modulus was a little higher in the larger-size fraction, although this fact does not appear to be very significant within the margin of experimental error, and may be due to a slightly higher bulk density of the specimens made with this fraction.

Toughness drops slightly on raising granule size (about 5%), a value that in reality is close to the margin of experimental error. If this outcome is compared with that of mechanical strength (which drops around 15% on going from the small-size to the large-size fraction), the inference can be drawn that the reduction in mechanical strength on raising granule size is basically due to the increase in flaw size.

This finding highlights the fact that tile mechanical strength can be raised in two different ways: by increasing toughness and decreasing microcrack size.

6. CONCLUSIONS

The results obtained in the present study allow drawing the following conclusions:

- Various methods were analysed for determining mechanical strength, Young's modulus and toughness. The methods that yield the best results are:
 - Mechanical strength and Young's modulus: 3-point bending (3PB)
 - Toughness: chevron notch method, notching with a disc.
- The toughness concept is applicable to the study of fracture in green ceramic bodies (dry and as-pressed).

- Mechanical strength, Young's modulus and toughness rise on raising tile bulk density and spray-dried powder moisture content. They therefore exhibit parallel behaviour.
- At a given bulk density, σ_R , E and K_{IC} increase with moisture content. This effect, predicted by fracture mechanics theory, was more pronounced in the case of K_{IC} .
- Microcrack size (fracture-initiating flaws), depends exclusively on tile bulk density, and decreases as this increases. This size is of a magnitude similar to that of the granules, which indicates the importance of granule size in mechanical strength.
- When different granule-size fractions are analysed, toughness is observed to virtually remain constant, while mechanical strength drops on raising granule size. This is a result of microcrack size growth on working with larger granules.
- The observation of fracture with an electronic microscope revealed that fracture was caused by various mechanisms, depending on pressing pressure and powder moisture content. At low pressures and moisture contents, intergranular failure prevails, whereas at high pressures and moisture contents, intragranular failure plays a greater role.

ACKNOWLEDGEMENTS:

The present study has been conducted in the project "Improvement of the Mechanical Properties of Green Tile Bodies" (no. BES2-5603), funded by the Commission of European Communities within the framework of the programme Industrial Technologies and Materials (Brite-Euram III). We should like to thank the Commission for the support received in conducting the work.

We should also like to thank the companies participating in the project: Arcillas Industriales y Transformaciones S.L (ARCITRAS); Atomizadora, S.A; Ceramco, S.p.a; Cerdomus Ceramiche, S.p.a.; Peris y Cia, S.A. (PERONDA); Tau Cerámica and Watts Blake Bearne & Company, plc (WBB), which have made it possible to develop the project.

7. NOMENCLATURE

a:	flaw or notch size [microcrack] (m)
a':	natural flaw size (m)
b:	specimen width (m)
D:	specimen diameter (m)
E:	Young's modulus (Pa)
h:	specimen thickness (m)
K_I :	stress intensity factor (Pa m ^{1/2})

K_{IC} :	critical stress intensity factor [toughness] ($\text{Pa m}^{1/2}$)
L :	specimen length (m)
m :	Weibull modulus
p :	load (N)
p :	pressing pressure (Pa)
p_S :	survival probability (probability of a tile not fracturing on applying a given load)
p_R :	breaking load (N)
s :	typical deviation
S :	span between bottom support rods [3 and 4-point bending] (m)
S' :	span between top load rods [4-point bending] (m)
V_E :	equivalent volume (m^3)
w :	pad width (m)
χ_p :	spray-dried powder moisture content (kg water / kg dry solid)
y :	deflection at the load application point (m)
Y :	dimensionless geometric factor
α :	ratio (flaw size)/(specimen thickness)
ρ :	bulk density (kg m^{-3})
σ_0 :	scale parameter for the Weibull equation (Pa)
σ_R :	mechanical strength (Pa)
σ_{R3PB} :	3-point bending strength (Pa)
σ_{R4PB} :	4-point bending strength (Pa)
$\sigma_{RD CD}$:	diametral compression strength with direct load application (Pa)
$\sigma_{RD CP}$:	diametral compression strength with load application via padding (Pa)